Journal of ELECTRONIC MATERIALS, Vol. 47, No. 10, 2018
https://doi.org/10.1007/s11664-018-6486-0

Characterization of La-Zn Substituted Co_2Y Hexagonal Ferrite

R. VINAYKUMAR,[1,2] JYOTI,[1,3] and JAPES BERA [1,4]

1.—Department of Ceramic Engineering, National Institute of Technology, Rourkela 769008, India. 2.—e-mail: vinaykumar.r1984@gmail.com. 3.—e-mail: 215cr2298@nitrkl.ac.in. 4.—e-mail: jbera@nitrkl.ac.in

La-Zn substituted $Ba_2Co_2Fe_{12}O_{22}$ (Co_2Y) hexagonal ferrite was synthesized using a conventional solid-state method with composition $Ba_{2-x}La_xCo_2Fe_{12-x}Zn_xO_{22}$, where x equals 0.0, 0.1, 0.3 and 0.5. The phase formation behavior and changes in the crystal structure of the substituted ferrite were investigated using x-ray diffraction (XRD) analysis. Accurate lattice parameters were evaluated through Rietveld refinement of the XRD pattern. XRD, as well as energy dispersive spectral analysis, showed the formation of a lanthanum iron oxide phase in $x = 0.3$ and 0.5 compositions. There was a small increase in unit cell volume with the substitution. The microstructural analysis showed a decrease in grain size with increasing substitution. The magnetic properties; M_s, M_r, and H_c of the ferrite were measured and found to increase with increasing substitution. Permittivity and permeability were measured and found in the range 10–16. It can be concluded that the La-Zn substitution was an effective method for improving magnetic and dielectric properties of the Co_2Y ferrite.

Key words: Co_2Y hexagonal ferrite, solid state reaction, La-Zn substitution, grain growth inhibitor, magneto-dielectric properties

INTRODUCTION

Hexagonal ferrites $Ba_2Co_2Fe_{12}O_{22}$ (Co_2Y) have been studied for different high-frequency applications such as antennae, microwave absorbers, and inductors because of their room temperature ferrimagnetic, dielectric and insulating properties.[1-4] The general formula of Y-type ferrite is $Ba_2Me_2Fe_{12}O_{22}$, where *Me* is a small divalent cation such as Zn, Co, Ni, Cu, etc. The crystal structure of hexagonal ferrite consists of different stacking sequences of hexagonal layers.[1-3] One molecular unit of Co_2Y ferrite consists of one S ($Co_2Fe_4O_8$) and one T ($Ba_2Fe_8O_{14}$) type building blocks. The S block consists of two spinel unit 2($CoFe_2O_4$) and T ($Ba_2Fe_8O_{14}$) block is made of four oxygen layers with Ba atom replacing an oxygen atom in the middle of two layers.[4] One unit cell of Co_2Y structure has three molecular formula units 3($Ba_2Co_2Fe_{12}O_{22}$), that is, 3(ST) blocks that are stacked along *c*-axis of the hexagonal structure. The structure has the space group R_3m.

At room temperature, Co_2Y ferrite has planar anisotropy with the preferred direction of magnetization in the hexagonal basal plane at 90° to the *c*-axis, which, however, changes to a cone of magnetization below − 58°C.[4] The anisotropy of Co_2Y ferrites is mostly attributed to the presence of the Co^{2+} ion in octahedral position. As the magnetization of Y type ferrite can rotate freely in plane/cone, they are good soft magnets due to the combination of high permeability, low coercivity and low magnetic losses at high frequency.[4]

Among different Y type ferrites, Zn_2Y has highest saturation magnetization (M_s = 42 A m^2 kg^{-1}) and Co_2Y has M_s of 34 A m^2 kg^{-1} at room temperature.[2,5] However, Co_2Y has highest magnetocrystalline anisotropy. The properties of Co_2Y ferrite can be changed by substituting Co with Zn. With the substitution of Zn, the magnetization of Co_2Y ferrite increases and the Curie temperature (T_c) decreases, as Zn weakens the superexchange interaction in the lattice. Similarly, the permeability of Co_2Y ferrite

(Received March 18, 2018; accepted June 27, 2018; published online July 6, 2018)

can be enhanced by forming a solid solution with Zn_2Y ferrite, which has higher permeability than Co_2Y.[6] The permittivity of $Co_{2-x}Zn_xY$ ferrite was also reported to increase with Zn substitution.[7]

The electromagnetic properties of hexagonal ferrites can also be changed by doping different transition and rare earth metals. La^{3+} substitution for Ba^{2+} (or Sr^{2+}) in different hexagonal ferrites have been reported.[8-11] Usually, trivalent La^{3+} and divalent Zn^{2+} are co-substituted for Ba^{2+} and Fe^{3+}, respectively, to compensate the electrical charges in the ferrites.[12-16] Although La-Zn co-substitution has been extensively studied for M type hexagonal ferrite, there are very few reports on this co-substitution in Y-type ferrites. Recently, Nejad et al.[17] reported that the magnetic property of Ni_2-Y ferrite increases with La-Zn co-substitution. To date, there is no report relating the effect of La-Zn co-doping on the properties of $BaCo_2Y$ ferrite. The present work focused on the synthesis and characterization of La^{3+}-Zn^{2+} co-substituted Co_2Y ferrites. The effect co-substitution on phase stability, changes in crystal structure, microstructure, magnetic and dielectric properties of substituted Co_2Y ferrites were investigated.

MATERIALS AND METHODS

La-Zn substituted Co_2Y ferrite; $Ba_{2-x}La_xCo_2Fe_{12-x}Zn_xO_{22}$ (x = 0, 0.1, 0.3, 0.5) powder was prepared by solid-state reaction. The raw materials $BaCO_3$, Fe_2O_3, CoO, La_2O_3, and ZnO were taken by the molar ratio and ball-milled for 12 h using propanol media. Milled powder was dried and calcined at 1050°C for 4 h to obtain the ferrite phase. The calcined powder was further milled for 12 h to obtain a fine particle size. The milled powder was granulated using 5 wt.% PVA solution as a binder. The granulated powder was pressed in the form of pellets (diameter 13 mm and thickness 2 mm) and toroids (inner diameter 3 mm, outer diameter 7 mm and thickness 2 mm) using a uniaxial press at a pressure of 4 tons. Finally, all pressed samples were sintered at 1150°C for 4 h.

The crystalline phase formed in the calcined specimen was identified by x-ray diffraction (XRD) using a Rigaku diffractometer (model; ULTIMA-IV/ Japan). Lattice parameters of substituted ferrites were refined by the Rietveld method using the program "materials analysis using diffraction" (MAUD),[18] considering the space group $R\ \bar{3}m$ (SG No 166). The microstructure was examined by a field emission scanning electron microscope (FESEM) equipped with energy dispersive spectrum (EDS) analyzer (FESEM; model Nova Nano SEM/ FEI). The magnetization behavior of the ferrite was measured using vibrating sample magnetometer (VSM; Lake Shore 7400 S) at a maximum applied field of 15 kOe and at room temperature. The saturation magnetization (M_s) was deduced by a model described by Grossinger[19] as per the equation:

$$M = M_s\left(1 - \frac{b}{H^2}\right) \quad (1)$$

Here M is magnetization, H is magnetic field applied, b is a constant related with magneto-crystalline anisotropy. M_s was calculated from the intercept of the straight line extrapolated in M versus $1/H^2$ plot for $1/H^2$ approaches zero. The initial permeability, permittivity, magnetic and dielectric losses, were measured by an LCR meter (model; Agilent E4982A) in the frequency range of 1 MHz to 1 GHz at room temperature. Before measurement, the LCR meter was calibrated using the 16195B calibration kit, which includes open, short, 50 Ω load, low-loss capacitors.

RESULTS AND DISCUSSION

Phase and Structural Analysis

Figure 1 shows Rietveld refinement output of unsubstituted Co_2Y ferrite XRD pattern. All peaks of the pattern were assigned to hexagonal ferrite phase $Ba_2Co_2Fe_{12}O_{22}$ and were indexed as per PDF card number 44-0206. XRD analysis was carried out to investigate the change in crystal structure of Co_2Y ferrite. Figure 2 shows the XRD patterns of different $Ba_{2-x}La_xCo_2Fe_{12-x}Zn_xO_{22}$ ferrites. All XRD data were taken on sintered pallet, but not on powder samples. For that reason, the intensities of 00l peaks were very large. For example, the peak at the angular position ~ 25° corresponds to the (0012) reflection of Y ferrite and the intensity of the peak was comparatively large due to the preferred

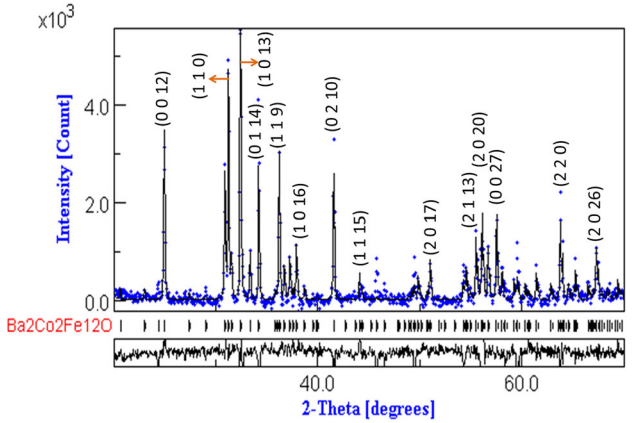

Fig. 1. Rietveld refinement output of $Ba_2Co_2Fe_{12}O_{22}$ ferrite XRD pattern, showing observed (+), calculated (solid line) XRD profile, their differences in the bottom and position of allowed Bragg reflections (tick marks) for the phase.

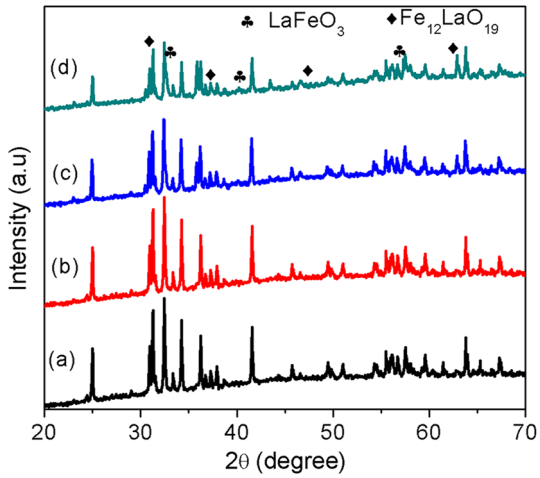

Fig. 2. XRD pattern of sintered $Ba_{2-x}La_xCo_2Fe_{12-x}Zn_xO_{22}$ ferrite with composition: (a) pure Co_2Y, $x = 0.0$, (b) $x = 0.1$, (c) $x = 0.3$, and (d) $x = 0.5$.

grain growth along the a–b plane of hexagonal ferrite. Accurate lattice parameters were evaluated through Rietveld refinement of XRD patterns. Lattice parameters (a and c), the volume of the unit cell, x-ray density of different compositions are shown in Table I. There was an increase in lattice parameters and volume of the unit cell in $x = 0.1$ composition. For compositions $x = 0.3$ and 0.5, no further change in lattice parameters was observed. A small increase in lattice parameter may be due to the substitution of Zn^{2+} with a larger ionic radius (0.82 Å) compared to Fe^{3+} (0.67 Å). A little amount of $Fe_{12}LaO_{19}$ and $LaFeO_3$ phases were identified in $x = 0.3$, and 0.5 specimens (Fig. 2c and d), which indicates that the La mainly forms lanthanum ferrite phases. However, no secondary phase corresponding to Zn has been found. Results show that the Zn is substituting Fe in ferrite lattice and the substituted iron reacts with La to form lanthanum ferrite phases.

Table I. Lattice parameters (a and c), the volume of the unit cell, and x-ray density ($d_{x\text{-ray}}$) with La-Zn content, x

x	a (Å)	c (Å)	Volume (Å^3)	$d_{x\text{-ray}}$ (g/cc)
0	5.896	43.74	1317	5.35
0.1	5.910	43.85	1326	5.32
0.3	5.911	43.84	1326	5.32
0.5	5.912	43.85	1327	5.33

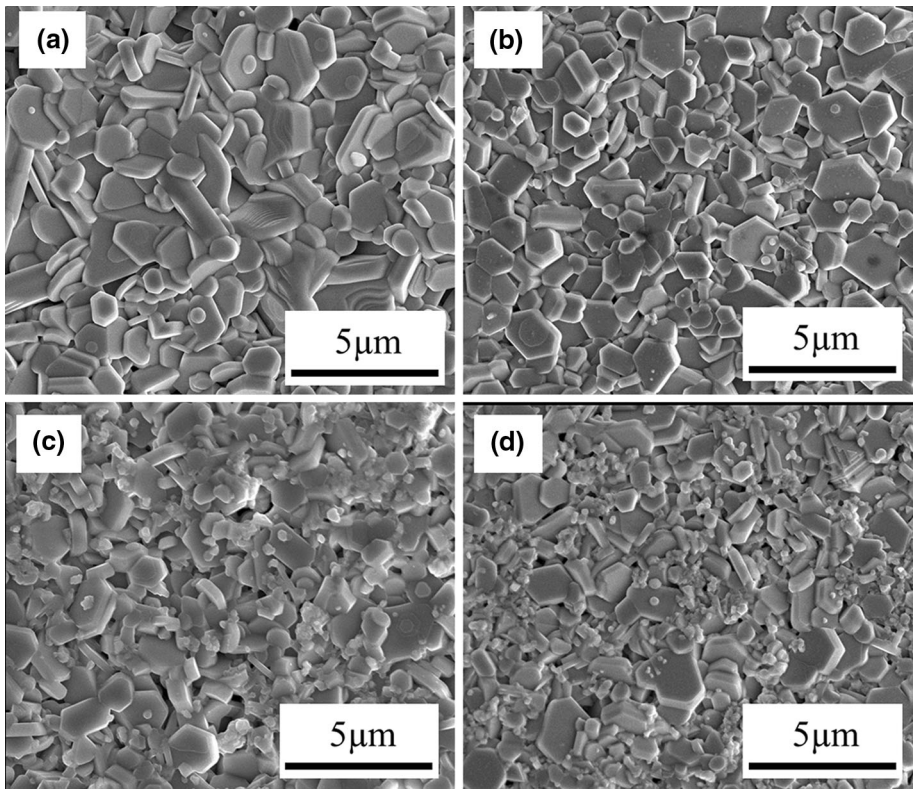

Fig. 3. SEM micrographs of $Ba_{2-x}La_xCo_2Fe_{12-x}Zn_xO_{22}$ ferrite with composition: (a) $x = 0.0$, (b) $x = 0.1$, (c) $x = 0.3$, and (d) $x = 0.5$.

Microstructure Analysis

Figure 3 shows FESEM micrographs of $Ba_{2-x}La_x$-$Co_2Fe_{12-x}Zn_xO_{22}$ ferrites. The micrographs show that all the specimens have the hexagonal plate-like grains, which is very common for hexagonal ferrites. Specimen with $x = 0.3$ and 0.5 composition show a duplex grain structure having the hexagonal plate-like grains with bigger size and some smaller grains in the grain boundary region. To identify the grain boundary phases, EDS analysis was carried out. The EDS analysis of hexagonal grains confirmed that the plates are composed of Zn substituted $BaCo_2Y$ ferrite phase and La elements were not found in hexagonal plates. However, La along with Fe and O elements were detected in the smaller grain, which suggests that La is not able to substitute inside the crystal structure of Co_2Y ferrite. The XRD phase identification also confirmed the formation of $Fe_{12}LaO_{19}$ and $LaFeO_3$ compounds. It is also observed that the grain size (hexagonal plates) decreases with increasing La-Zn substitution. La in the form of La-Fe oxide phase resides at the grain boundary of the ferrite phase, which inhibits the grain growth of the ferrite.

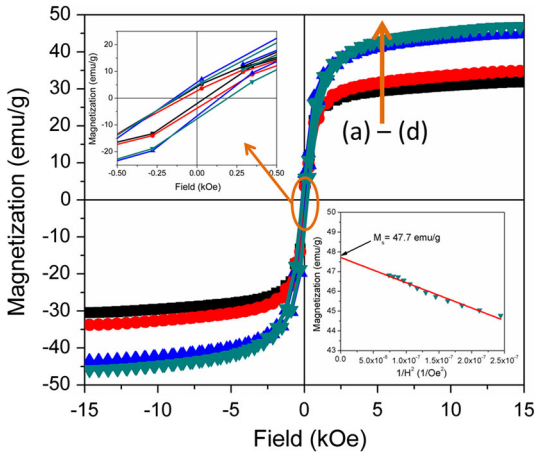

Fig. 4. Magnetic hysteresis loops as a function of applied field measured at room temperature for the $Ba_{2-x}La_xCo_2Fe_{12-x}Zn_xO_{22}$ ferrite with composition: (a) $x = 0.0$, (b) $x = 0.1$, (c) $x = 0.3$, and (d) $x = 0.5$. The insets show the details of saturation region and the plot of M as a function of $1/H^2$ for $x = 0.5$ composition.

Magnetic and Dielectric Properties

Figure 4 shows the variation of magnetization (M) as a function of applied field (H) for $Ba_{2-x}La_x$-$Co_2Fe_{12-x}Zn_xO_{22}$ ferrite. The magnetic properties such as coercive field (H_c) and remanence magnetization (M_r) were determined directly from the hysteresis loops. The saturation magnetization (M_s) was obtained from the intercept of the straight line of the M versus $1/H^2$ plot (Inset of Fig. 4) as per Eq. 1. Table II summarizes the magnetic properties of different composition. The values of the M_s, M_r and, H_c of the ferrite specimen were found to increase with the increase in La-Zn substitution. For example, the unsubstituted Co_2Y ferrite showed the M_s of only 32 emu/g compared to 47.7 emu/g found in $x = 0.5$ composition, which is due to the increase in Zn substitution concentration. It is known that Zn^{2+} ions occupies the tetrahedral site in spinel structure and forces Fe^{3+} ion to the octahedral site where the octahedral and tetrahedral sites are coupled antiparallel. The Y-type ferrite is composed of S and T blocks. In spinel type S block, there are four octahedral and two tetrahedral magnetic moments in opposite spin, giving a total magnetic moment of 2 in that block.[4] As the Zn^{2+} ion resides in the tetrahedral site, the amount of opposite magnetic spin at tetrahedral site decreases and the resultant magnetic moment in S block increases. Thus Zn substitution enhances the magnetization in the Co_2Y ferrite and similar results were also reported earlier.[20,21] The values of H_c were found to increase with increasing substitution, which may be due to the decrease in ferrite grain size with La increasing concentration. With the decrease in grain size, the domain-wall movement decreases and hence coercivity increases.[8,9,17]

The electromagnetic properties are essential for many high-frequency applications of hexagonal ferrites, particularly in integrated chip components. The properties of interest are resistivity, permittivity, and permeability, which in general should be as high as possible for the high-frequency application. Table II summarizes the permittivity (ε), dielectric loss (tan δ_ε), initial permeability (μ') and magnetic loss tangent (tan δ_μ) of La-Zn substituted Co_2Y ferrite measured at a frequency 100 MHz. Figure 5 shows the frequency dependency of ε and tan δ_ε in

Table II. Saturation magnetization (M_s), remanence magnetization (M_r), coercivity (H_c) and permittivity (ε), dielectric loss (tan δ_ε), initial permeability (μ'), and magnetic loss (tan δ_μ) at 100 MHz for different $Ba_{2-x}La_xCo_2Fe_{12-x}Zn_xO_{22}$ ferrite compositions

x	M_s (emu/g)	M_r (emu/g)	H_c (Oe)	(ε)	(tan δ_ε)	(μ')	(tan δ_μ)
0	32	3.6	70	14.6	0.002	10.3	0.003
0.1	33.1	5.3	110	15.3	0.008	10.8	0.005
0.3	45.9	7.2	160	16.1	0.038	11.2	0.017
0.5	47.7	7.3	205	16.2	0.025	12.1	0.003

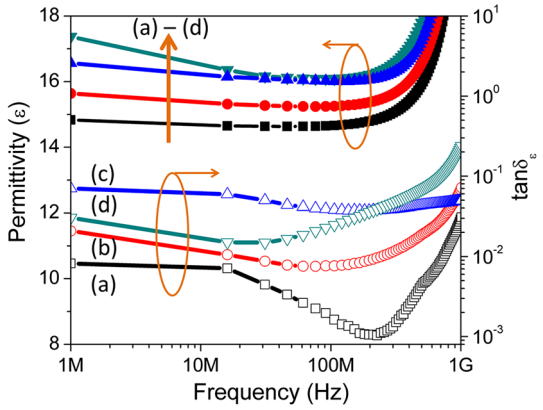

Fig. 5. Frequency dependency of permittivity (ε) and dielectric loss tangent (tan δ_ε) for $Ba_{2-x}La_xCo_2Fe_{12-x}Zn_xO_{22}$ ferrite with composition: (a) x = 0.0, (b) x = 0.1, (c) x = 0.3, and (d) x = 0.5.

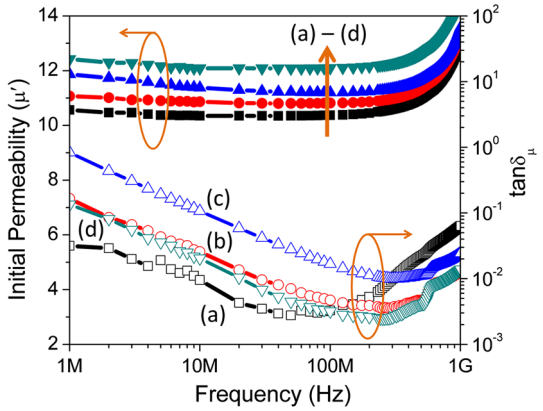

Fig. 6. Frequency dependency of initial permeability (μ') and magnetic loss tangent (tan δ_μ) for $Ba_{2-x}La_xCo_2Fe_{12-x}Zn_xO_{22}$ ferrite with composition: (a) x = 0.0, (b) x = 0.1, (c) x = 0.3, and (d) x = 0.5.

the frequency range 1 MHz to 1 GHz. The ε is the dielectric polarization arises in the ferrite due to the formation of diploe between metal cation and oxygen ion. The ε is stable up to about $\sim$ 300 MHz, and above that frequency, there is an increase in permittivity due to the ferroelectric resonance/relaxation processes, where the frequency is not being responded by the material. Figure 5 also shows that ε increases with increasing La-Zn substitution. The tan δ_ε increases with La-Zn substitution due to the increase in ε. Increase of the dielectric constant can be explained on the basis of the polarization process in ferrites. With the substitution of Zn^{2+} ions, some of the Fe^{3+} ions of tetrahedral sites are forced to migrate to the octahedral sites, which may enhance the dipole moment of the spinel block.

Figure 6 shows the frequency dependency of μ' and tan δ_μ in frequency range 1 MHz to 1 GHz. Here again, the μ' increases with increasing Zn substitution. Usually the saturation magnetization and magnetic anisotropy determine the initial permeability of ferrite. It is known that Zn substitution in Co_2Y ferrite leads to the decrease in magnetic anisotropy and increase in saturation magnetization.[20,21] Thus increase in μ' is due to the increase in saturation magnetization as stated above. The μ' is also stable up to about 300 MHz. The tan δ_μ values were low both in pure and substituted Co_2Y ferrites.

CONCLUSION

La-Zn co-substituted $Ba_{2-x}La_xCo_2Fe_{12-x}Zn_xO_{22}$ (x = 0.0, 0.1, 0.3 0.5) ferrite was successfully synthesized through solid state reaction route. A small amount of lanthanum iron oxide secondary phase was found along with major Co_2Y ferrite phase in compositions; x = 0.3 and 0.5. There was a small increase in the volume of the unit cell due to the higher ionic radius of Zn^{2+} ion than the Fe^{3+} ion. There was a decrease in the grain size with increase in La-Zn substitution due to the presence of lanthanum iron oxide phase at the grain boundary, which inhibits the grain growth. The saturation magnetization also increased with the increase in La-Zn substitution due to the preferential occupancy of the nonmagnetic Zn^{2+} ion at the tetrahedral site. The values of H_c were found to increases due to the decrease in grain size. In the La-Zn substituted Co_2Y ferrite, permittivity and permeability were found in the range 14–16 and 10–12 respectively and both were stable up to $\sim$ 400 MHz. The La-Zn substituted Co_2Y ferrite is proposed for high-frequency microwave applications due to its improved magnetic and dielectric properties.

ACKNOWLEDGEMENTS

This work was supported by the SERB-DST (Grant No. SB/S3/ME/076/2013) of Government of India. Also, authors would like to acknowledge Dr. Prakash Nath Vishwakarma, Department of Physics and Astronomy, NIT Rourkela for the help on measuring the magnetic properties of the samples.

REFERENCES

1. G.H. Jonker, H.P.J. Wijn, and P.B. Braun, *Philips Tech. Rev.* 18, 145 (1956).
2. J. Smit and H.P.J. Wijn, *Ferrites* (The Netherlands: Philips Technical Library, 1959).
3. M. Sugimoto, *Ferromagnetic Materials*, vol. 3, ed. E.P. Wohfarth (Amsterdam: North-Holland Physics Publishing, 1980), p. 394.
4. R.C. Pullar, *Prog. Mater Sci.* 57, 1191 (2012).
5. M. Obol and C. Vittoria, *IEEE Trans. Magn.* 39, 3103 (2003).
6. Y. Bai, J. Zhou, Z. Gui, and L. Li, *Mater. Sci. Eng. B* 103, 115 (2003).
7. M. Wu, H. Zhang, X. Yao, and L. Zhang, *J. Phys. D* 34, 889 (2001).
8. X. Niu, Y. Liu, M. Li, B. Wu, and H. Li, *J. Electron. Mater.* 46, 7 (2017).
9. T.T. Loan, T.T. Viet Nga, N.P. Duong, S. Soontaranon, and T.D. Hien, *J. Electron. Mater.* 46, 6 (2017).
10. Y. Wang, L. Li, H. Liu, H. Qiu, and F. Xu, *Mater. Lett.* 62, 2060 (2008).

11. D. Seifert, J. Topfer, F. Langenhorst, J.M. LeBreton, H. Chiron, and L. Lechevallier, *J. Magn. Magn. Mater.* 321, 4045 (2009).
12. H. Taguchi, T. Takeshi, and K. Suwa, *J. Magn. Soc. Jpn.* 21, 901 (1997).
13. Z.H. Hua, S.Z. Li, Z.D. Han, D.H. Wang, M. Lu, W. Zhong, B.X. Gu, and Y.W. Du, *Mater. Sci. Eng. A* 448, 326 (2007).
14. J. Bai, X. Liu, T. Xie, F. Wei, and Z. Yang, *Mater. Sci. Eng. B* 68, 182 (2000).
15. J.C.C. Huacuz and G.M. Suarez, *J. Magn. Magn. Mater.* 242–245, 430 (2002).
16. D.U. You-wei, L.U. Huai-xian, Z. Yu-cheng, and W. Ting-xiang, *J. Magn. Magn. Mater.* 31–34, 793 (1983).
17. E.H. Nejad, Y.A. Farzin, and M.A. Heydari, *J. Magn. Magn. Mater.* 423, 226 (2017).
18. http://www.ing.unitn.it/~maud/.
19. R. Grossinger, *Phys. Stat. Sol. A* 66, 665 (1981).
20. C.M. Kim, C.H. Rhee, and C.S. Kim, *IEEE Trans. Magn.* 48, 11 (2012).
21. S. Bierlich and J. Topfer, *J. Magn. Magn. Mater.* 324, 1804 (2012).